Graphene/aluminum oxide interfaces for nanoelectronic devices

V-B Vu, Jean-Luc Bubendorff, L Mouafo, S Latil, A Zaarour, J-F Dayen, Laurent Simon, Y Dappe

Graphene/Aluminum oxide interfaces for nanoelectronic devices

V.-B. Vu[1], J. L. Bubendorff[2], L.D.N. Mouafo[3], S. Latil[1], A. Zaarour[2], J.-F. Dayen[3,4], L. Simon[2], Y.J. Dappe[1]

[1] SPEC, CEA, CNRS, Université Paris-Saclay, CEA Saclay, 91191 Gif-sur-Yvette Cedex France.
[2] Institut de Sciences des Matériaux de Mulhouse, CNRS-UMR 7361, Université de Haute Alsace, 68093 Mulhouse, France.
[3] Université de Strasbourg, CNRS, Institut de Physique et Chimie des Matériaux de Strasbourg (IPCMS), UMR 7504, 23 rue du Loess, Strasbourg, 67034, France.
[4] Institut Universitaire de France, 1 rue Descartes, 75231 Paris cedex 05.

Keywords: graphene, nanoparticule, single electron transistor, heterostructure, nanoelectronics, multifunctional materials.

Abstract: In this work, we study theoretically and experimentally graphene / aluminum oxide interfaces as 0D/2D interfaces for quantum electronics as the nature of the interface is of paramount importance to determine the quantum transport. Indeed, the electronic transport is driven either by a channel arising from a strong hybridization at the interface, or by tunneling across a van der Waals interface. By combining electronic spectroscopy and scanning microscopy with Density Functional Theory calculations, we show that the interface is of weak and van der Waals nature. Quantum transport measurements in a single electron transistor confirm this result. This work paves the way to new atomic environment control in single electron device.

1. Introduction

Graphene is now well known as a fantastic playground for probing electronic properties and potential new devices for future nanoelectronics. Its semimetallic character combined to its high carrier mobility makes it a very good candidate for quantum electronic transport [1]. As such, many recent developments in electronics and spintronics have been achieved involving

interfaces with graphene. For example, combination with other two-dimensional materials like *h*-BN or transition metal dichalcogenides (TMDCs) through van der Waals heterostructures have been widely studied [2-4]. In these systems, since the interaction is very well-known (weak and van der Waals interactions), there is no ambiguity about the combination of electronic properties of the different materials. It simply consists in aligning the Fermi level of each layer, without hybridizing the electronic states due to the spatial van der Waals gap between the layers [5]. In that respect, these 2D/2D van der Waals interfaces are well-known now.

The realization of other graphene-based hererostructures involving an insulating layer (ex. Al_2O_3, MgO,…) was first motivated by the realization of top gate for Graphene Field effect Transistor application (GFET)[6], but rapidly graphene was considered both as an electrode in a tunneling junction and a substrate supporting the heterojunction, mainly for spintronic applications [7]. In the case of GFET, the insulating layer needs to be thick (hundreds of nanometer) to avoid the leakage current. Contrarily, in the case of tunneling junction the thickness of the insulating decoupling layer should be of two orders of magnitude lower. By looking for the condition of growth of thinner insulating layer, as we will see later, islands with core-shell structures instead of the initially expected continuous 2D layer have been observed, opening the way to mixed dimensional van der Waals heterostructures [8]. In such hybrid systems, metallic core can be used as a Coulomb island, while the insulating shell provides the right electronic coupling condition for single electron transport [3,4]. Most of these studies concern quantum transport properties, revealing for example the mechanism of Coulomb and magneto-Coulomb blockade. However, the nature of the interface is still under debate, and truly physico-chemistry characterization of the 0D/2D interface is still lacking. To the best of our knowledge, there is only one experimental paper which reports hard X-ray photoelectron spectroscopy technique to characterize aluminum oxide/graphene interface in the case of a thick oxide for Graphene based FET [9]. We have found no reference addressing the problem of 0D

cluster, the interface, how the graphene layer is modified in the vicinity and in between the 0D structure and how this interface may depend on the graphene (G) /substrate interface. This is the purpose of the present multidisciplinary study.

Here we consider aluminum oxide clusters deposited on graphene as 0D/2D interfaces for quantum electronics. We compare systematically different types of graphene layer: graphene on SiO_2, G/Ni and well-oriented G/SiC(0001). The main goal of this work is to determine experimentally and theoretically the nature of the interface, namely whether we have a strong hybridization between aluminum oxide and graphene, opening an electronic gap in graphene or if we have an interface comparable to a van der Waals heterostructure with potential graphene doping. In the first case, the newly created channel in the graphene gap through hybridization of electronic states would drive the electronic transport, whereas in the second case, the electronic current would tunnel through the spatial van der Waals gap, resulting in very different transport signatures. To this end, using X-ray and angular resolved photoemission spectroscopy (XPS and ARPES) for electronic properties and scanning electronic, atomic force and scanning tunneling microscopy (SEM, AFM and STM) for structural aspects, combined to Density Functional Theory (DFT) calculations, we have fully characterized aluminum and aluminum oxide /graphene interfaces. Finally, transport measurements have been performed to illustrate one of the case of study, and confirm the experimental and theoretical results of the interface characterization.

2. Results and discussion

2.1. Al-AlOx/graphene interfaces preparation and characterization

The procedure of the formation of AlOx Quantum Dots (QD) for the sample dedicated to transport measurements consists in the evaporation of Aluminum (typically with a thickness of 2nm) by an oxidation in air. Initially the Al layer thickness was chosen to synthetize a continuous oxidized Al layer as a 2D tunneling barrier. Counterintuitive results lead to the

observation of QD. In this experimental section, we would like to address the question of the formation of the Aluminum oxide QD and more particularly the nature of the interface with the graphene as a function of the supporting substrate and its influence on the graphene band structure.

We first reproduce and compare the oxidation at air of 2nm Al evaporated on CVD G/SiO_2 (provided by Graphenea®) and G/Ni(111), two types of G/substrate system similar to those for which Coulomb blockade was observed [3,4]. The samples (pristine graphene) were cleaned with annealing in UHV at temperature below 500°C in order remove surface contamination and residual oxidation of the graphene.

Figure 1 shows the evolution of the C1s core level peak measured by X-ray photoelectron spectroscopy using a monochromatized Al $K_{\alpha 1}$ source (1486.6 eV) for both system, pristine graphene, after the deposition of Al and after oxidation in air for 15 min (the process that was initially used for device fabrication). The resulting Al_2p core level peak is also given for G/Ni and G/SiO2 in Fig. 1. D) and H) respectively. In the case of G/Ni in Fig. 1 A the best fit was obtained with a Doniach Sunjic form convoluted with a Gaussian line shape and a FWHM of 0.71 eV. After evaporation of Al (Fig. 1 B) adding a second component at 286.3 eV is necessary to fit the C1s core level peak. After oxidation in air (Fig. 1 C),

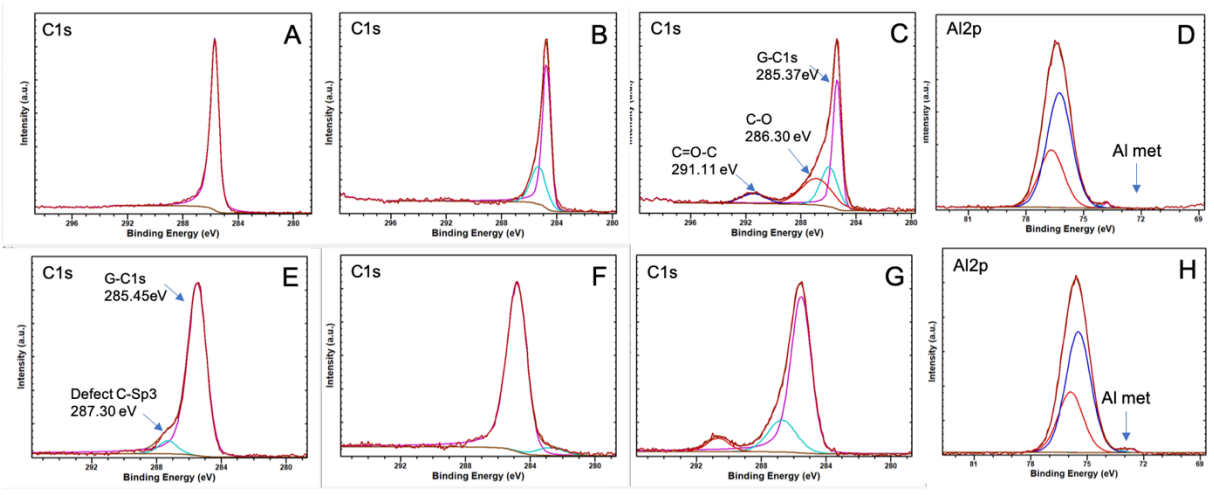

Figure 1 : C1s core level peak of pristine Graphene, after evaporation of 2 nm Al, and 15min oxidation at air for G-Ni (A, B, C) and CVD-G/SiO_2 sample (E, F, G) and corresponding Al2p core level peak in both system (D and H).

two supplementary components are observed. Such components could be attributed to defect (sp^3 character bond) or C-O. In the present case this cannot be attributed to C-Al (around 282eV) or C-O-Al (284 eV) bonds as these should lead to core level peak at lower binding energies than the sp^2-G component [10,11]. A C-O bond is possible as we never obtained pure Al without spontaneous oxidation during the transfer of sample and the analysis in spite of a relatively low pressure during the deposition (5.10^{-9} mbar).

In Figure 1 E to G, we show the same evolution for a G-CVD on SiO2. In Fig. 1 E, the pristine graphene shows a usual component at 287.3 eV attributed to grain boundaries defects. This component disappears after Al deposition (Fig. 1 F) and a small feature centered at 282.77 eV can be attributed to C-Al bonds. After the oxidation in air (Fig. 1 G), this feature disappears and we can observe, as for G-Ni in Figure 1 C) two supplementary components at 286.71 and 290.66 eV that can be attributed to C-O and C=O-C bonds respectively.

The Al_{2p} core level peaks after oxidation are given in Figure 1 D and H. Most of the Aluminum is oxidized but not fully and it remains 1.7% of Al metallic in both cases. As we will see later, we have a core-shell structure with a metallic core surrounded by Al_2O_3 and sub oxide. In such a configuration, the signal intensity of the core level peak Al_{2p} attributed to Al is probably underestimated by the effect of burying of the metal atoms under the Al_2O_3 shell.

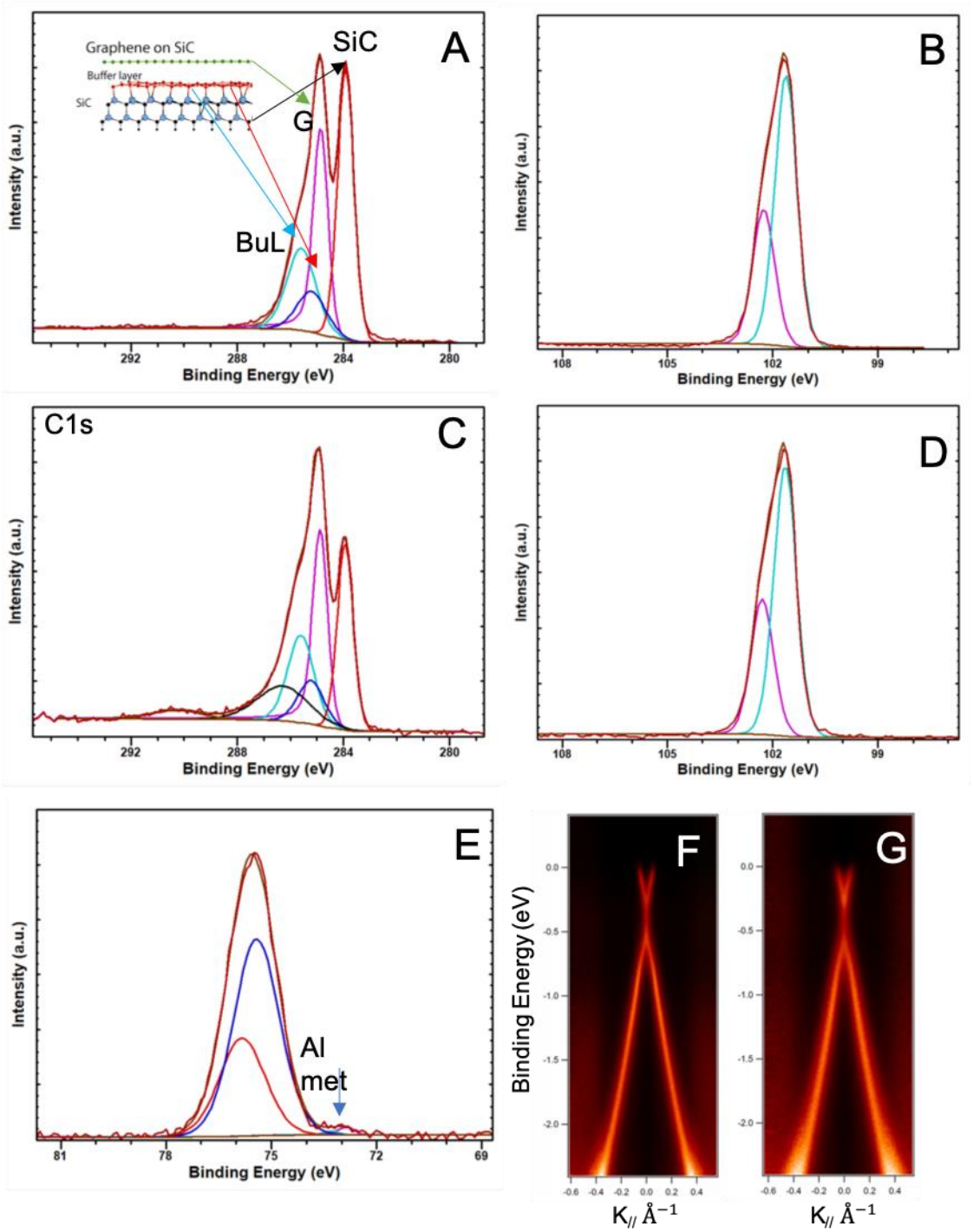

Figure 2: C1s (A and C) and Si2p (B and D) core level peak of 2nm Al deposited on G-SiC(001) and oxidized 15 min at air). The resulting Al_{2p} peal after oxidation is given in E. F and G compare two band dispersion measured around K point (along the direction K'-K-K') with a non-monochromatized UV- lamp 40.6 eV and using an electron detector Scienta R-3000.

In Figure 2 we have used a well-defined and controlled G-SiC(0001). This graphene layer is obtained by the annealing of SiC(0001) subtrates at high temperature under UHV (up to 1200°C). This annealing leads to the exo-diffusion of silicon atoms from the SiC substrate, leading to the formation of the so-called Buffer layer (BuL) which is a monolayer G (MLG) partially covalently bonded to the silicon atoms of the substrate. Depending on the annealing temperature and time, one, two or more graphene layer in van der Waals interaction are obtained [12]. The graphene layers are well oriented and we can measure the band dispersion using Angle-Resolved Photoemission Spectroscopy (ARPES) in addition to the X-ray photoelectron spectroscopy measurements (XPS) for the characterization of physico-chemical nature of the interface.

Figure 2 A and C show the C1s core level peaks on pristine graphene and after the oxidation of 2nm Al at air for 15 min. In Fig. 2 A we identify four components on the C1s core level peak. One at 283.93 eV is attributed to carbon atoms of the SiC substrate, the top graphene layer gives a component at 284.85 eV and the BuL leads to two components S1-sp^3 at 285.21 eV and S2-sp^2 at 285.6 eV. After oxidation in Figure 2 B) all component corresponding to the pristine graphene are preserved and we see, as for the previous samples two components at 286.27 and 290.25 eV that we have attributed to Carbone oxidized species. The ratio of intensity between G-C1s and S1, S2 components is unchanged in the deconvolution, which ascertains no modification of the interface G/SiC. The Si_{2p} core level peak before and after the process of Al deposition and oxidation are also unchanged (Figure 2 B and D respectively). As for the previous samples in Fig. 2 E, the Al_{2p} peak shows a fully oxidized Al_2O_3 but with a remaining metallic Al component (1.7% in area). The advantage of G-SiC(0001) system is the well-orientated G layer which allows us to perform ARPES measurements. In Figure 2 F and G, we show the dispersion and well-known Dirac cone measured around the K point before (on

pristine graphene) and after Al deposition and oxidation in air respectively. There are identical and the deposition and the oxidation had no effect on the graphene band structure.

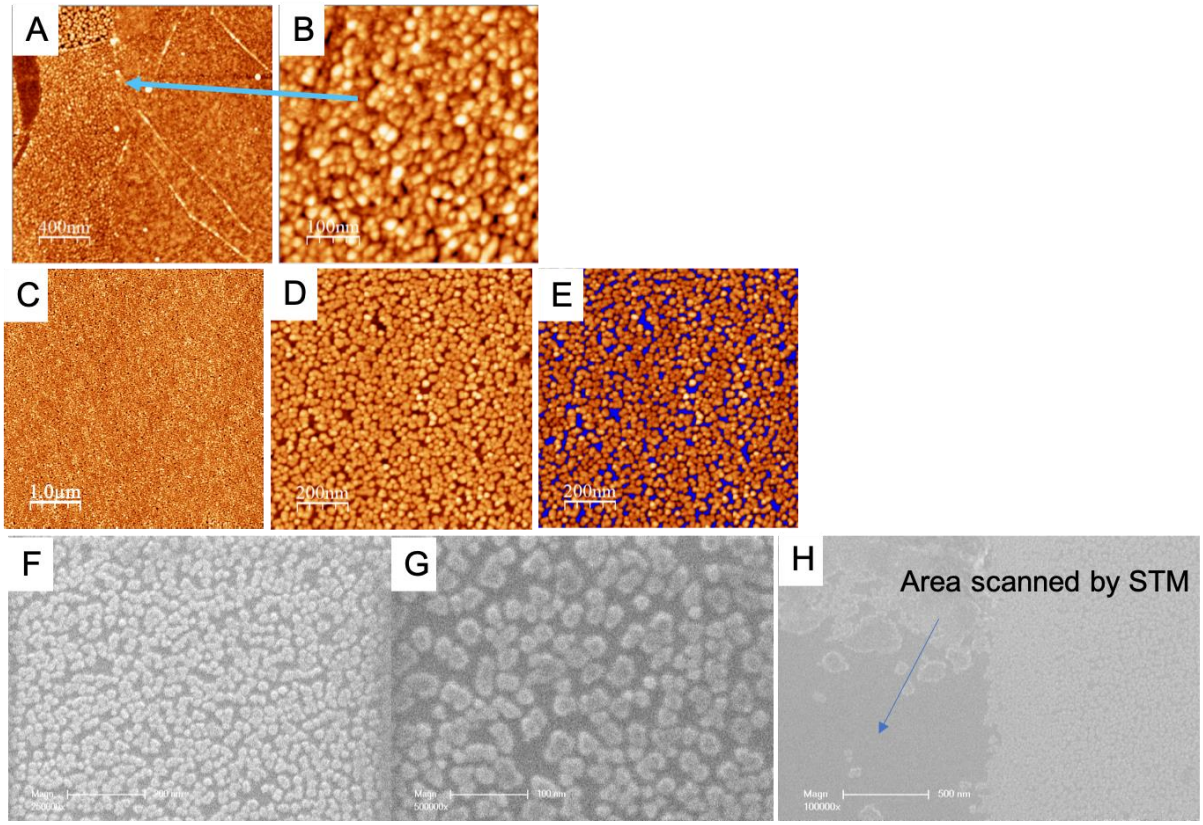

Figure 3: Atomic force microscopy (AFM) image of 2nm Al oxidized 15 min at air for CVD-G/SiO2 (A-B) and G-SiC(001) (C-D). In E the flooding analysis shows the basal plane of Graphene surface uncovered with QD. In F, G and H SEM images (JEOL JSM7200) of the same sample. In H a 10µm x10µm area without QD correspond to a scanned area with the Scanning Tunneling Microscope (STM) and QD in van der Waals interaction removed by the tip as discussed in the text.

In Figure 3 we show typical Atomic Force Microscopy (AFM) images of 2nm oxidized Al on CVD-G (A and B) and on G-SiC (0001) (C and D). We observe highly homogeneous spreading of islands. This suppose that the initial deposition of Al was homogeneous and the oxidation created this structure. These islands have an average diameter of 20±1 nm and high of 12nm on G-SiC substrate. The image in Fig. 3 E is a flooding analysis of Fig. 3 D with the high histogram. On the 1µm x 1µm the island recovers 89.50% of the surface. Then the graphene area free of

islands is 10.5% of the surface. Due to the low inelastic mean free path of electron (typically less than 1nm for ARPES measurements), it is clear that the dispersion given in Figure 2 G corresponds to the graphene free area and certainly not to graphene under the island. We can conclude that the graphene under the island is not perturbed. SEM images done with a Jeol JSM7200. In Figure 3 F and 3 G, we see the islands and the free area around. We also observe a modification of the contrast inside the QD which relates the change of conductivity of the island. We think that this reveals the core-shell character of these structures. More interestingly in H) we show a clean smooth surface, a graphene free area of 10µm x10µm, which corresponds to the largest scanned area that we used with our Omicron-LT-STM. We tentatively tried to image these islands in UHV after oxidation, the images were unstable and it was not possible to get any reproducible image even at low current (down to 100pA) and high bias (few V), the condition expected to be able to get stable STM images on such a system. We finally found out, with this SEM image that the tip has swept and clean the surface by removing the islands. This shows that the islands are probably in van der Waals interaction with the graphene.

Let us come back to the observation of the two unknown components attributed to C-O and C=O-C observed after the oxidation. The first simple explanation of the presence of these components is that we have a carbon contamination during the processes of oxidation in air. To test this hypothesis, we have mounted a new UHV chamber connected on our set-up. Well-prepared and cleaned graphene surface in Ultra-High Vacuum conditions can be transferred in a chamber allowing an oxidation from few Langmuir ($1L=10^{-6}$ torr.s), with exposition in the range of 10^{-6} mbar up to 100 mbar of O_2 pressure. The chamber is then pumped again and sample are transferred in the analysis chamber without breaking the vacuum. With this set-up, it is possible to follow the first step of oxidation up to atmospheric pressure of oxidation avoiding any contamination.

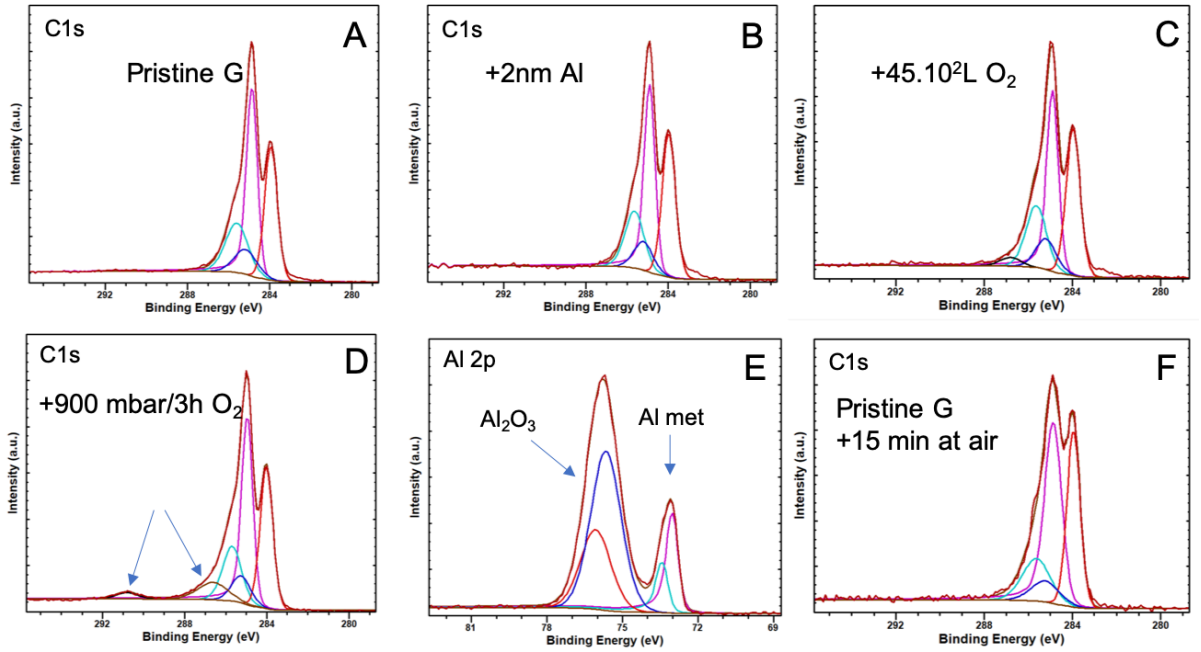

Figure 4: C1s evolution of graphene on SiC(0001), in A for pristine, B after deposition of 2nm Al, C after the exposure of 45.10^2 L of dry O_2, D with exposure of 900mbar O_2 for 3h. The resulting Al_{2p} core level peak after this last exposure is given in E. IN F, the C1s of a "standard", pristine G-SiC(0001) simply oxidized at air for 15 min.

We have followed step by step the oxidation process by recording the C1s, Si_{2p} and Al_{2p} core level peaks. We have cumulated O_2 exposure for 45.10^2L, 45.10^3L and $45.\ 10^4$L and then $7\ 10^8$ L, 8.10^9L, 5.10^{11} L and $7.3\ 10^{12}$L (1L=$1.33\ 10^{-6}$ mbar/s). The last one corresponds to an exposition of 900mbar O_2 during 3h.

Figure 4 A shows the C1s core level XPS spectra recorded at grazing angle on the pristine ML graphene on SiC(0001). We observe the four components already discussed in Figure 2. After Al deposition the C1s core level peak in Figure 4 B does not change. In Figure 4 C, the first exposition gives rise to the emergence of a faint C-O component at 286.9eV.

This component increases in intensity and the second one at 290.8eV attributed to C=O-C appears only after the fifth exposition. The resulting C1s core level peak after the last exposure is given in Figure 4 D. In Figure 4 E, we see that the Al layer is not fully oxidized even after

such an exposure at 900mbar O_2 for 3h (7.3 10^{12}L) which is 7 x10^6 higher than 15 min at air (1.2x10^6 L).

This experiment shows unambiguously that the components are not due to a contamination. A second hypothesis is to attribute this component simply to the oxidation of the graphene. Figure 4 F shows the C1s core level peak of a pristine G-SiC(0001) simply oxidized at air for 15 min. We see no new component and the graphene layer is not oxidized with the exposure time even at atmospheric pressure.

It seems that Al does not react with the graphene layer (*i.e.* carbide with Al-C bonds), it forms an oxide Al_2O_3 but allows a reaction with the graphene to creates oxidized species C-O and C=O-C for the higher exposure. Such decomposition is certainly catalyzed by the Al/Al_2O_3 core shell QD.

We also notice that even huge dry O_2 exposure is not sufficient to fully oxidize the 2nm Al layer and the presence of H_2O (wet-oxidation) is certainly necessary in this oxidation process leading to the formation of QD.

The graphene band structure is not modified by the QD at least in between, and we found out that their interaction with the graphene are very weak and supposed to be in van der Waals interactions. However, we cannot exclude the formation of defects on the graphene layer itself at the Al_2O_3 interface.

2.2. Theoretical characterization of Al/graphene and AlOx/graphene interfaces

In this section, we aim at theoretically characterizing the interface between graphene and aluminum or graphene and aluminum oxide. The main objective here is to determine whether these interfaces are of weak or covalent nature. Indeed, the nature of the interface has strong implications on its electronic transport properties. As such, its perfect understanding is a requisite to explain the transport measurements on this system. Following the experimental

characterization from the previous section, we attempt to model these interfaces using Density Functional Theory (DFT) calculations. However, since the exact structure at the interface is not known, it is difficult to consider a full aluminum or aluminum oxide surface in contact with graphene. Therefore, we have chosen to consider the interaction of a single AlO_2 molecule on graphene. This situation corresponds to the first step of aluminum deposition and oxidation on graphene, as described in the experimental procedure of the previous section. Calculations have been performed using the very efficient localized-orbital basis set Fireball [13]. Optimized basis sets for C, O and Al have been used, in agreement with previous calculations [14]. Hence, we have considered a 4x4 layer of graphene, with periodicity in the *xy*-plane, and an AlO_2 molecule on top. The structure has then been fully optimized for different initial AlO_2/graphene distances, until the forces went below 0.01 eV/Å. In addition, in order to observe a particular effect of graphene deformation, which could induce a specific bonding with the aluminum dioxide molecule, we have performed these calculations by varying the lattice vectors of the graphene unit cell. In other words, we simulate the compression or extension of the graphene plane.

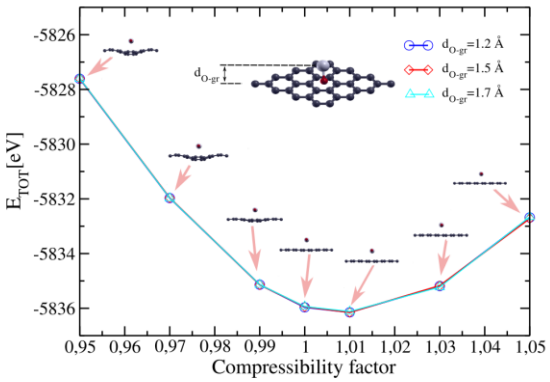

Figure 5: evolution of the total energy of the AlO_2/graphene interface calculated in DFT, as a function of the compressibility factor of graphene. The corresponding optimized structures are superposed to the energy curve and the initial separation distances are indicated in inset.

The corresponding evolution of the total energy of the AlO_2/graphene interface as a function of the graphene compressibility factor is presented in Figure 5. The initial unit cell is shown in inset as well as the initial oxygen/graphene distances. As a result, we can observe that the minimum of energy corresponds to a slight extension (about 0.01%) of the graphene plane, but overall that the interaction is weak, driven by van der Waals interaction.

Since these first calculations have been performed considering a specific angle of the AlO_2 molecule with respect to graphene, we have repeated the procedure for other angles. In particular, we show the same result with a rotation of 60 degrees of the molecule with respect to graphene in Figure 6. In this configuration, we observe again a minimum of energy for a slightly strained graphene, but the interaction remains weak and van der Waals. Also, for a compression factor of about 0.03 %, we can observe an important deformation of graphene and a covalent bonding of the molecule. However, despite the stronger energy associated to a covalent bonding, the important deformation of the graphene sheet prevents the system to minimize its energy. In order to fully explore this energy landscape, we have repeated the procedure considering several rotation angles, ranging from 0 to 90 degrees.

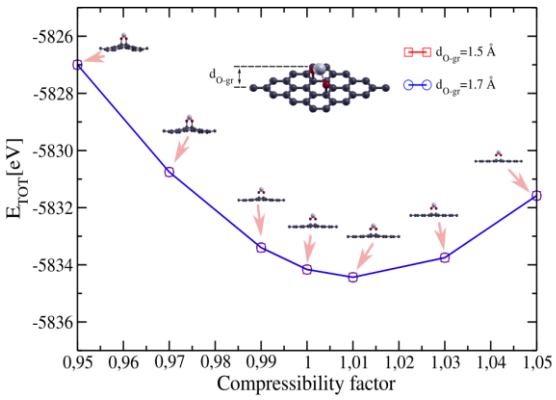

Figure 6: evolution of the total energy of the AlO_2/graphene interface calculated in DFT, as a function of the compressibility factor of graphene. The corresponding optimized structures are superposed to the energy curve and the initial separation distances are indicated in inset.

The corresponding energy variation for two different graphene compression factors is represented in Figure 7.

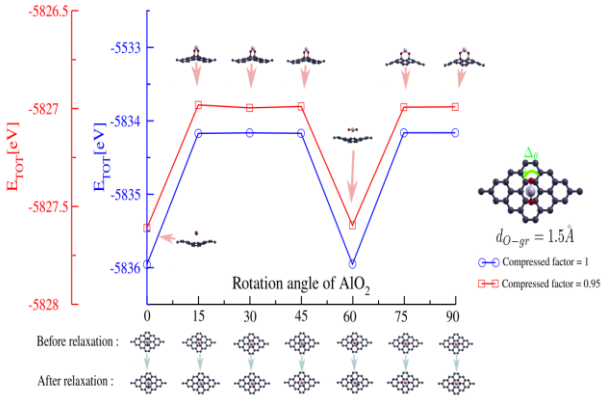

Figure 7: evolution of the total energy of the AlO_2/graphene interface calculated in DFT, as a function of the rotation angle of the AlO_2 molecule with respect to graphene. The blue curve corresponds to an unstrained graphene plane, whereas the red curve corresponds to a compression factor of 0.05 %. The corresponding optimized structures for the compressed graphene are superposed to the red energy curve and the initial separation distance as well as the initial atomic configuration are indicated in inset.

From this Figure, we can observe that the energy minima are located at 0 and 60 degrees, corresponding to a 60-degree periodicity in the rotation, which is consistent with the hexagonal symmetry of the graphene network. Moreover, these minima do not depend on the compression factor, only their amplitude varies according to the graphene deformation. This is also consistent with the fact that graphene deformation has an energetic cost that prevents the system to minimize its energy. As such, the red energy curve corresponding to the compressed graphene is higher than the blue energy curve corresponding to the unstrained graphene. Finally, and this is the most interesting for our study, we can observe that all the configurations correspond to a covalent bonding of the AlO_2 molecule on graphene, except the two minima in 0 and 60 degrees, which correspond to van der Waals interaction. Also, we have performed similar calculations considering several AlO_2 molecules in interaction deposited on graphene, which has led to the same result, namely a van der Waals interaction at the interface.

Consequently, from these results, we can deduce that the interaction between aluminum oxide and graphene is of weak nature, leading to a van der Waals barrier between both.

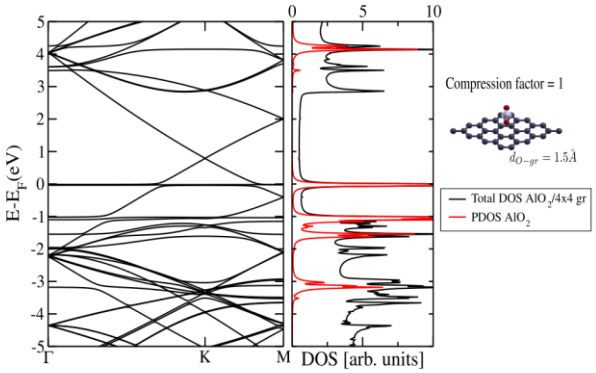

Figure 8: bandstructure (left), total DOS of AlO_2/graphene and AlO_2 PDOS (right) calculated in DFT for a minimal configuration at zero angle and an unstrained graphene plane. The corresponding atomic structure is represented in inset.

From these weak interacting configurations, we have now calculated the electronic structure of the interface. Hence, we represent in Figure 8 the bandstructure of the AlO_2/graphene interface, in the 4x4 graphene unit cell. One can clearly see the Dirac cone at the K point, located at around 0.8 eV above the Fermi level. This corresponds to a charge transfer from graphene to the AlO_2 molecule, leading to a p-doping of graphene. This charge transfer is estimated to be around 0.5 electron per unit cell. We can also observe the AlO_2 molecular states, which correspond to non-dispersive states in the bandstructure, since the molecule is not hybridized with graphene. Also in Figure 8, we represent the total Density of States (DOS) of the interface (in black) as well as the projected DOS (PDOS) of the AlO_2 molecule (in red). The molecular gap lies around 4 eV and the Lowest Unoccupied Molecular Orbital (LUMO) is located at the Fermi level, which is in agreement with the important charge transfer from the graphene to the molecule. Finally, we show in Figure 9 the electronic structure of two AlO_2 molecules adsorbed

on graphene. The corresponding unit cell has been fully optimized following the procedure of the previous calculations.

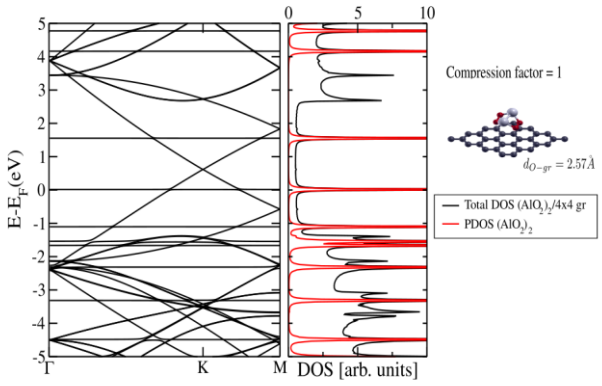

Figure 9: bandstructure (left), total DOS of two AlO_2 molecules on graphene and two AlO_2 PDOS (right) calculated in DFT for a minimal configuration at zero angle and an unstrained graphene plane. The corresponding atomic structure is represented in inset.

In this configuration, we can also observe a p-doping of graphene, but less pronounced than with one adsorbed molecule. Namely, the Dirac cone is located at around 0.5 eV above the Fermi level. This means that there is still a charge transfer from graphene to the two AlO_2 molecules, but less important than for one single molecule. From our calculations, this charge transfer is estimated around 0.3 electrons per unit cell. In the same manner, the molecular gap is around 1.7 eV, with the LUMO still pinned at the Fermi level. From these results, we can infer that the formation of a layer of aluminum oxide will decouple this layer from graphene, leading to a smaller charge transfer and a reduction of the electronic gap at the interface.

Consequently, these simulations show that the deposition of aluminum followed by oxidation on graphene leads to the formation of a small van der Waals heterostructure between graphene and aluminum oxide, with charge transfer from graphene to aluminum oxide, inducing a p-doping in graphene.

2.3. Transport measurements

In this last section, we report experimental study of low temperature charge transport in 2D-0D heterostructures based on graphene/Al clusters implemented into vertical field effect transistor archiecture. The devices are obtained in tow steps, following the synthesis process previously described in [4,15]. First, an ultra-thin film (1nm nominal thickness) of Al is e-beam evaporated onto the surface of CVD graphene, which play the role template for the growth of the Al nanoclusters. Then, self-limited oxidation in controlled atmosphere is performed, resulting in a core-shell structure with metallic Al core embedded in an alumina oxide shell. This unique architecture enables the simple fabrication of a three-terminal vertical field-effect-transistor geometry (Figure 10 a).

Typical source-drain current-voltage characteristics measured at low temperature (1.5 K) are shown in Figure 10 b. The Isd-Vsd traces present clear features of sequential single-electron tunneling. First, a sharp conductance gap is measured at low bias in the vicinity of zero voltage, resulting from the Coulomb blockade experienced by the electrons when tunneling from the electrode to the central metallic core through the alumina tunnel barrier. From the Coulomb gap, we can estimate the Coulomb charging energy to be around 70 meV, corresponding to clusters of typically 6 nm metallic core (estimates done using a simple cylindrical capacitor model), in good agreement with structural characterization studies [4,15]. As V_{SD} is further incremented, a first, second and more tunneling thresholds are reached, opening additional conductance channels through supplementary resonant levels of higher energy, which manifest by Coulomb staircase features in the I_{SD}-V_{SD} trace. The corresponding differential conductance curves reveal well-defined narrow Coulomb oscillations (Figure 10.c). Each peak represents a threshold from n to n+1 electrons currents flowing through the device. Notice that the robust single-electron processes and the rather good agreement with the simple orthodox theory model

indicate that the electron transport relies on the selection of preferential conductive channel though the best coupled Coulomb island.

We also explored the transconductance properties of the 2D-0D in three terminals configuration. To do so, we use the $Si(P+)/SiO_2$ for the implementation of a back electric gate. Because of its single atom thin structure and low density of states, the graphene is partially transparent to a vertical electric field. This enables to electrically tune the density of states of the Coulomb Island through the graphene, and to explore the implemention of a three-terminal vertical single electron transistor (SET). While such degree of control was recently demonstrated in MoS2 based 2D-0D vertical SET [3], it is not obvious how the transparency of graphene will be high enough to reproduce this concept.

We investigate in Figure 10 d the gate control of the single electron features in a typical graphene based 2D-0D three terminals devices. The low temperature Isd(Vg) trace measured at fixed Vsd present an semi-periodic oscillatory behavior characteristic of gate control in single electron transistor. The Gate dependent current oscillations in our 2D-0D heterostructure can be understood by considering that the applied Vg does not only modulate the energy band occupation of the graphene flake. It also tunes the electric state of the metallic core of the NPs standing on the Gr surface. Incrementing the gate voltage linearly shifts the chemical potential μ of the NPs and consequently their discrete Coulomb levels. Any time a discrete CB state enters the dc-bias window |eVs| defined by the source-drain potential difference, a single electron current flows through the device resulting to an 'on state'. In the contrary, when no CB state is located within such window shifted out by V_G, no current flows. The device is in the 'off state'. It results an oscillatory logic gate behavior of the current typical to single electron transistor. The background signal is resulting from thermal assisted tunneling through the oxide barrier.

These results extends the concept of 2D-0D vertical SET to graphene based channel,

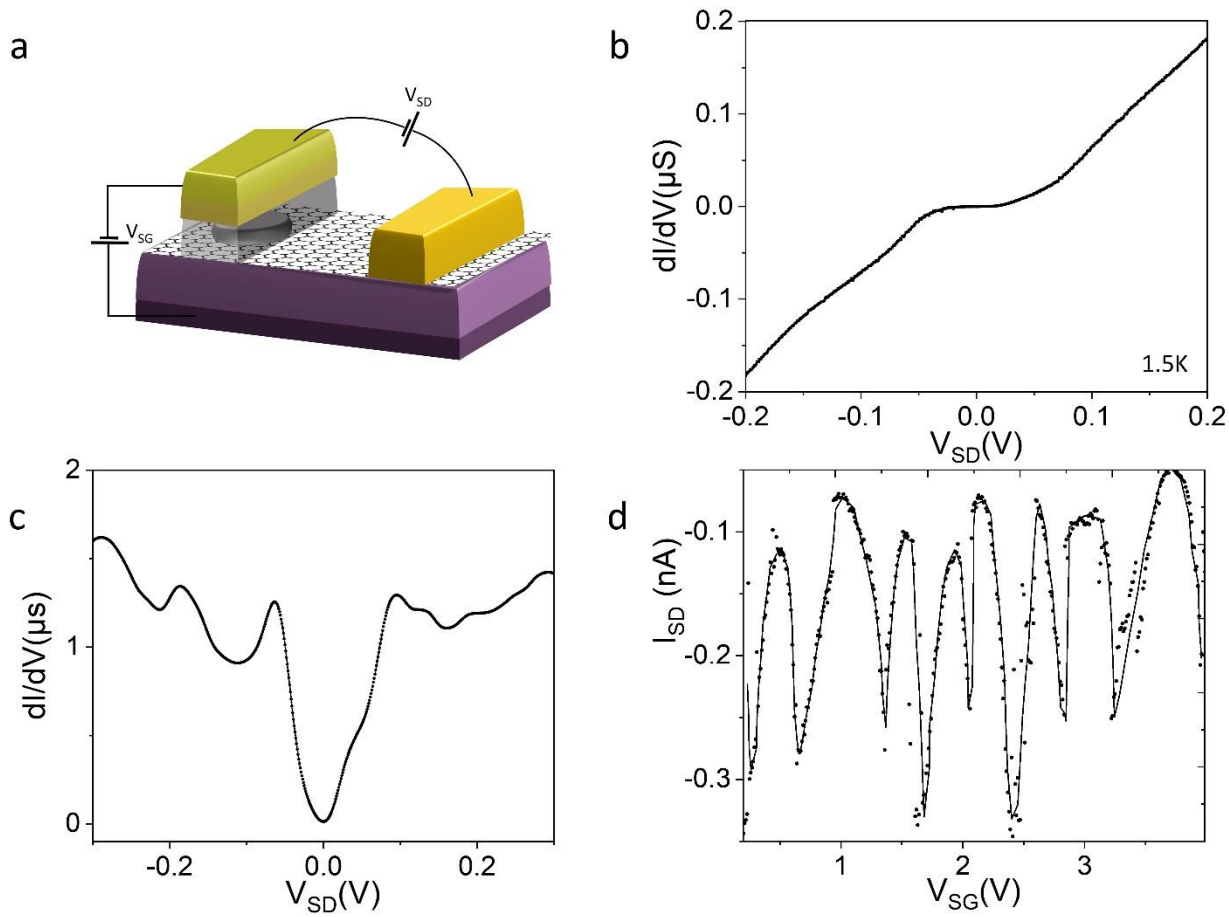

demonstrating the robustness and versatility of this architecture to a wider class of materials than transition metal dichalcogenides. The possibility to combine graphene, known for its high mobility and long spin coherence time, with single electron quantum islands, opens the doors for exploring original architectures of single-electron spintronics devices.

Figure 10: Low temperature single-electron transport. A. Schematic of a vertical single-electron transistor built from 2D-0D heterostructure. b. Current-voltage source to drain measurements ($I_{SD}(V_{SD})$ performed at 1.5K on a typical graphene/aluminum cluster 2D/0D heterostructure. Coulomb staircase features can be observed. c. Derivative conductance of the $I_{SD}(V_{SD})$ trace better highlighted the Coulomb thresholds. d. Single-electron transconductance demonstrating Coulomb oscillations arising from electrostatic gate control, throughout the graphene template, of the Al Coulomb island chemical potential.

Conclusion

In conclusion, we have studied the interface core-shell aluminum oxide 0D structure with a graphene plane on different substrates, SiO_2 in the case of CVD graphene, Ni and G on SiC(0001). Thorough physical-chemistry studies show that the clusters are in van der Waals interaction. The uncovered free Graphene layer between the clusters is also unperturbed without effect of doping and gap opening as clearly revealed by ARPES measurement. The graphene layer acts as a perfect electrode, which also flows the charges and balances the potential between the clusters as expected by the transport measurement. This property is independent of the substrate on which the graphene is deposited or synthetized and the present study strongly shows that this is only due to the process of the formation of the cluster, the growth of aluminum on the graphene and the mechanism of the oxidation. These results are validated experimentally by implementing a prototype of Single Electron Transistor, based on the aluminium/graphene 0D/2D hybrids. These results open new avenues to control at the atomic level the environment of Coulomb island in the search of scalable and optimized single electron device.

Further studies will specifically address the question of the selectivity of cluster in the transport measurement, the exact nature of the core-shell structure (the thickness ratio of the oxide/and the Al core) by combining conductive AFM and Pulse-force mode measurement.

Acknowledgements

We acknowledge the financial support by MIXES (grant ANR-19-CE09-0028).

References

[1] Andrea C. Ferrari *et al.*, Nanoscale 2015, 7, 4598.

[2] G. Fiori, F. Bonaccorso, G. Iannaccone, T. Palacios, D. Neumaier, A. Seabaugh, S.K. Banerjee, L. Colombo, Nat. Nanotechnol. 2014, 9, 768−779.

[3] L. D. N. Mouafo, F. Godel, L. Simon, Y. J. Dappe, W. Baaziz, U. N. Noumbé, E. Lorchat, M.-B. Martin, S. Berciaud, B. Doudin, O. Ersen, B. Dlubak, P. Seneor, and J.-F. Dayen, Adv. Funct. Mater. 2021, 31, 2008255.

[4] L. D. N. Mouafo, F. Godel, G. Melinte, S. Hajjar-Garreau, H. Majjad, B. Dlubak, O. Ersen, B. Doudin, L. Simon, P. Seneor, and J.-F. Dayen, Adv. Mater. 2018, 30, 1802478

[5] A. K. Geim and I. V. Grigorieva, Nature 2013, 499, 419.

[6] E. Guerriero, P. Pedrinazzi, A. Mansouri, O. Habibpour, M. Winters, N. Rorsman, A. Behnam, E. A. Carrion, A. Pesquera, A. Centeno, A. Zurutuza, E. Pop, H. Zirath and R. Sordan, Scientific Reports 2017, 7, 2419

[7] B. Dlubak, M-B. Martin, C. Deranlot, B. Servet, S. Xavier, R. Mattana, M. Sprinkle, C. Berger, W. a. De Heer, F. Petroff, A. Anane, P. Seneor and A. Fert, Nature Physics 2012, 8 (7) 557

[8] D. Jariwala, T. J. Marks and M. C. Hersam, Nature Materials 2017, 16, 170–181

[9] Y. Tateno , F. Mitsuhashi, M. Adachi, T. Yonemura, Y. Saito, Y.Yamamoto and T. Nakabayashi, Japanese Journal of Applied Physics 2020, 59, 124001

[10] G. Greczynski, D. Primetzhofer and Lars Hultman Applied Surface Science 2017, 436 102-110

[11] F. C. Liu, P. Dong, W. Lu, K. Sun Appl. Surf. Sci. 2019, 466, 202

[12] Y. Girard, S. Benbouabdellah, O. Chahib, C. Chacon, A. Bellec, V. Repain, J. Lagoute, Y. J. Dappe, C. González, W.-B. Su, Carbon 2023, 208, 22

[13] J. Lewis, P. Jelinek, J. Ortega, A. Demkov, D. Trabada, B. Haycock, H. Wang, G. Adams, J. Tomfohr, E. Abad, H. Wang, D. Drabold, Phys. Status Solidi B 2011, 248, 1989–2007

[14] M. Basanta, Y. Dappe, P. Jelínek, J. Ortega, Comput. Mater. Sci. 2007, 39 (4), 759–766

[15] F. Godel, L. D. N. Mouafo, G. Froehlicher, B. Doudin, S. Berciaud, Y. Henry, J.-F. Dayen, and D. Halley, Adv.Mater. 2017, 29, 1604837